Macromolecular Bioscience
www.mbs-journal.de

Multilayered Microneedles for Triphasic Controlled Delivery of Small Molecules and Proteins

*Nathaniel Wright, Tim Wu, and Yadong Wang**

Transdermal delivery is an attractive delivery method that increases bioavailability, is suitable for a wide variety of therapeutics, and offers stable delivery outcomes. However, many therapeutics are unable to readily cross the stratum corneum. Microneedles mechanically disrupt the cutaneous barrier to deliver small molecules, proteins, and vaccines. To date, microneedles have not been used in conjunction with coacervate, a liquid–liquid phase separation that protects unstable proteins. A three-layer microneedle for the controlled release of three different molecules is designed. Through micromolding, microneedles are efficiently generated, which benefits product scalability. The microneedles have good mechanical integrity and effectively penetrate porcine skin ex vivo. The three layers, in the microneedles, release the cargo in a three-phase manner. The released protein maintains its structure well. Moreover, layer thickness can be controlled by varying fabrication parameters. The microneedles can incorporate both small molecule drugs and protein therapeutics, thus promising uses in multi-drug therapies through a single treatment.

1. Introduction

Transdermal delivery has several advantages over oral delivery, the most common form of delivery for small molecules.[1] Transdermal delivery systems improve patient compliance, drug bioavailability, and reduce side effects partially due to the decreased peak release rates achieved.[2–4] Only small and nonpolar molecules can readily cross the skin barrier. Alternative approaches are needed for large or polar drugs. Passive methods of diffusion such as lipid encapsulation or chemical enhancement work by increasing the flux of compounds across the skin barrier.[3,5] Active methods including iontophoresis, sonophoresis, electroporation, or microneedling that either disrupt the normal barrier function of the epidermis or drive the passage of therapeutics across the stratum corneum.[2,5–7] Delivery of both proteins and small molecules has been achieved using these methods but often not simultaneously or in a single treatment. Given that microneedles can deliver a diverse range of molecules and proteins with a large variety of viable polymers, we chose to pursue this avenue of delivery.

Microneedles are micron-sized needles that mechanically disrupt the stratum corneum, forming pores for the delivery of therapeutics into the underlying skin layers.[2,8–10] The different types of microneedles, solid, hollow, coated, and dissolvable microneedles, enable variable drug delivery profiles and release kinetics giving greater user control over pharmacokinetics.[2,8,11] Within these categories, decisions about the materials and geometry of the microneedle itself are prudent in generating a sophisticated delivery vehicle for the needs of the user.[8] This flexibility offers more materials and drug combinations increasing the potential treatments available. Our microneedle patch was developed to incorporate multiple therapeutics in a facile manner. This layered system provides a simple method for the addition of different classes of drugs within solvent systems that are tunable based on the desired outcomes. With each layer being distinct, multiple release curves are achieved from a single microneedle patch, the timescale adjustable for the treatment strategy. For ease of communication, the first layer of the microneedle refers to the outermost layer that would first contact the tissue, with subsequent layers located closer to the center. These advancements improve ease of use of microneedles and allow for the development of many fine-tuned systems for disease treatments. This work can be used in conjunction with vaccines, protein therapies, or other multidrug treatment for improved outcomes.

2. Results

2.1. Morphology and Skin Penetration of Multilayered Microneedle

To examine the structural and morphological integrity of the layered microneedles, scanning electron microscope (SEM) images were obtained (**Figure 1**). These images demonstrated that the resultant needle structure replicates the pattern of the 3D-printed master molds. The SEM images showed the individual layers from the printing process. With these results, further analysis and characterization of the microneedle patch were completed.

The ability to penetrate the skin layer is key to the function of microneedles. Penetration is a product of many factors such

N. Wright, T. Wu, Y. Wang
School of Biomedical Engineering
Cornell University
Kimball Hall 290, Ithaca, NY 14853, USA
E-mail: yw839@cornell.edu

The ORCID identification number(s) for the author(s) of this article can be found under https://doi.org/10.1002/mabi.202300431

DOI: 10.1002/mabi.202300431

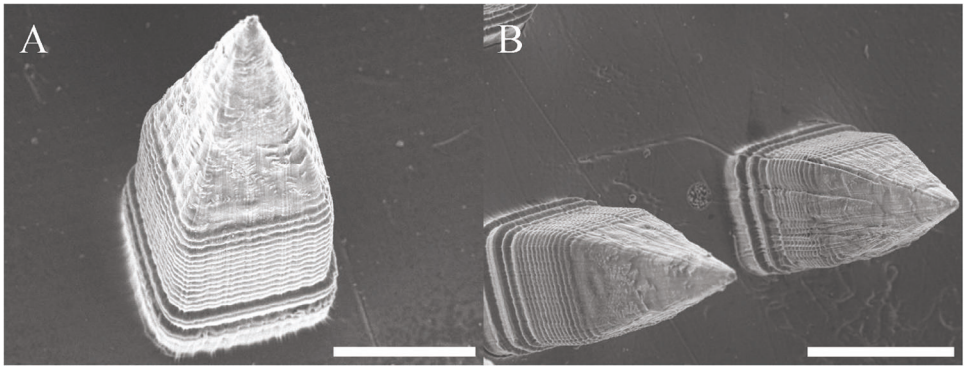

Figure 1. SEM Images of Multilayered Microneedle Patch: Fabricated microneedles were sputter coated prior to performing SEM. Images displayed show the layered lines that were generated during the 3D printing of the microneedle master molds. A) Scale Bar: 200 µm. B) Scale Bar: 300 µm.

as microneedle geometry and material choice.[12] We applied a three-layered microneedle to the pig skin by thumb pressure for 1 min. The first layer of the microneedle was made of carboxymethyl cellulose (CMC) which contained methylene blue, a second layer of ethyl cellulose (EC), and a third polyvinylpyrrolidone (PVP) layer. The microneedles were then removed, the skin imaged with a light microscope, and the image captured using an Excelis camera (**Figure** 2A,B). The microneedles displayed distinct penetration for the individual needles and were able to successfully deliver methylene blue into the skin. H&E stained porcine skin showed microneedle penetration (Figure 2C). Additionally, the microneedles imaged after skin insertion showed excellent structural integrity with minor damage and bending of the needle tips (Figure 2D,E). Dissolution of the first layer was also seen 10 min after insertion (Figure 2F). Further analysis of the microneedles was completed using an Instron for analysis of the mechanical properties of the microneedles (Figure 2G).

2.2. Control of Individual Layer Thickness

Through the adjustment of the amount of material used within the microneedle molds, the layer thickness can be modulated (**Figure 3**). Both CMC and EC were used for the first layer of microneedles. The inner dimensions of the void, that was left after filling of the microneedle, were measured for different volumes used. CMC filled the molds more than EC at or above 120 µL of polymer solution. CMC filled the molds to a similar extent as EC at other measured values. The volumes used were chosen by their ability to completely cover the mold and allow for complete needle formation through the patch. Special care was taken so that material would not be lost by avoiding an excessive volume on top of the microneedle molds prior to degassing.

2.3. Timed Release of Loaded Dyes from Layered Microneedle

Microneedles were fabricated with three different fluorescent molecules, fluorescein, methylene blue, and tetramethylrhodamine (TRITC) conjugated IgG in the first, second, and third layers, respectively. With the backing layer sealed, the microneedles were placed in water to simulate the sink conditions of the subcutaneous environment[13]. The microneedles showed a multi-phasic release profile for each of the molecules, with control dependent on which layer the molecules were in and the material used for encapsulation (**Figure 4**). This is seen by the burst release of fluorescein from the first layer composed of CMC. The second layer containing methylene blue in ethyl cellulose demonstrated a controlled release over days. Additionally, this second layer slowed the release of TRITC labeled antibody from the final layer of PVP resulting in controlled release over the course of a week.

2.4. Bioactivity of a Released Model Drug and Preservation of Protein Secondary Structures

Using microneedles either loaded with all-trans retinoic acid (ATRA), sodium butyrate (NaBu), or calcipotriol (Cal), RAW 264.7 cells, a macrophage cell line, were treated and then stimulated with lipopolysaccharide (LPS). Following incubation with LPS, NO produced by the cells was measured using the Griess Assay. The overall effect of ATRA, NaBu, and Cal showed the ability to downregulate the inflammatory response of macrophage culture demonstrating the functionality of the layered microneedles in vitro. In **Figure 5** the significance of both groups is shown between those with and without anti-inflammatory treatment. Retinoic acid was shown to be more potent in inhibiting the NO production of these macrophages compared to the effect of Cal or NaBu alone. Cal showed a stronger dose dependence curve than the other two molecules that were tested, where NaBu seemed to not be as potent as the other two small molecules tested.

To examine the secondary structure of the proteins, circular dichorism (CD) was used, before incorporation into the microneedles, and after release. The CD spectra showed the structural integrity for bovine serum albumin (BSA), lysozyme, and IgG were maintained in the microneedle and the fabrication process did not alter protein secondary structure (**Figure 6**). These proteins were chosen for their diverse sizes and for potential therapies. To best quantify these results, the measurements were processed in BeStSel. This program was used to determine the characteristics of the protein secondary structure that is seen in the wavelengths of 200–250 nm. The resultant measurements showed no significant difference between the control and proteins that were

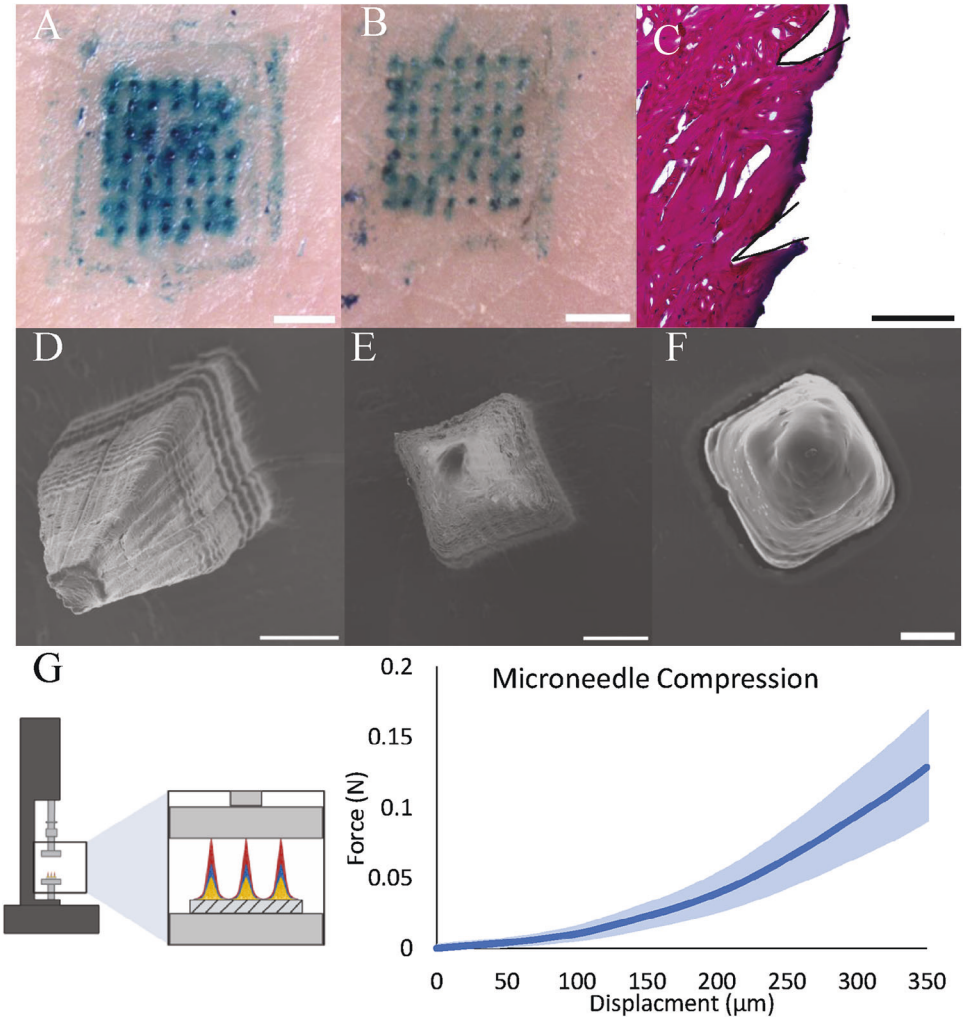

Figure 2. Microneedle Penetration of Porcine Skin: Microneedles were fabricated with methylene blue in the first layer of CMC and subsequent layers of EC and PVP that contained no dyes. A,B) Microneedles were applied to porcine skin and optical images taken of separate microneedle applications. Scale bar: 2 mm. C) H&E staining was performed on microneedle pierced skin, black is placed to show microneedle skin disruption. Scale bar: 100 µm. D–F) SEM images of microneedles after removal from pig skin. Scale bar: 100 µm. G) Mechanical testing of layered microneedles with corresponding graph of force applied over distance.

encapsulated and then released from the microneedles. This suggests that the secondary structure of the proteins remains intact after encapsulation. Thus, the protein function likely remains intact.

3. Discussion

Microneedles have previously been designed to achieve various needs of controlled release systems. Past work has demonstrated the release of levonorgestrel, as contraceptive agent, over a 30 day time period from a polylactic acid /poly(lactic-co-glycolic acid) microneedle.[14] Chitosan microneedles showed the release bovine serum albumin as a model protein over an 8 day period with CD confirming protein stability after encapsulation.[15] Insulin loaded microneedles were fabricated to be sensitive to hypoxic environment for a biologically responsive system.[16] Delivery of immunotherapeutics across the skin to target specific sites has also been explored.[17] Microneedles have also demonstrated great potential for vaccine delivery, for COVID-19, and other viruses.[18,19]

Many biological processes are enabled by multiple signaling molecules and often in stages that are disease specific. There is a need to deliver several therapeutic agents sequentially.[20,21] However, there is a lack of controlled release in multiple phases using microneedles, we sought to design a novel multiphase therapeutic delivery microneedle system. This would be beneficial to many diseases, such as melanoma, for more robust responses seen in multi-therapeutic treatments. To this end we developed a multi-layered microneedle capable of controlled delivery and encapsulation of multiple classes of therapeutics.[22] This microneedle patch can deliver small molecules and proteins to better optimize and facilitate the treatment of complex diseases requiring several therapeutics for optimal outcomes.

The quality of microneedle patch fabrication was examined by SEM. Microneedles satisfied the minimum force to pierce skin.[23] Layer failure was not observed upon skin penetration

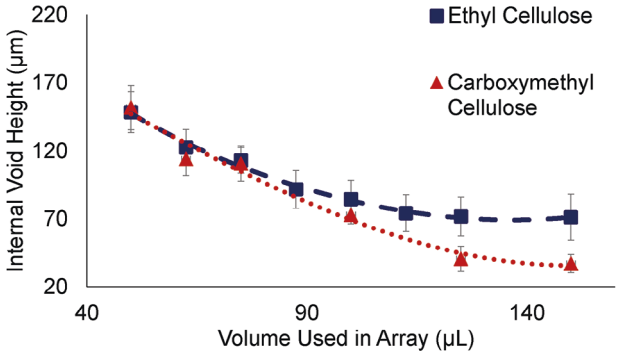

Figure 3. Varying Microneedle Layer Thickness through Modulating the Volume. Microneedles were fabricated with varying amounts of material (volume), the internal void was then measured. Carboxymethyl cellulose and Ethyl Cellulose were the two polymers used for this study.

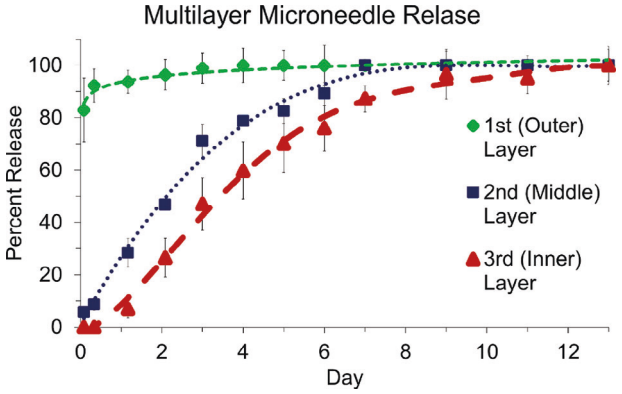

Figure 4. Microneedle release from a three-layered microneedle comprised of carboxymethyl cellulose, ethyl cellulose, and polyvinylpyrrolidone loaded with either fluorescein, methylene blue, or TRITC labeled IgG, respectively, simultaneously. The back was sealed, and the release profiles were measured over time using a spectrophotometer.

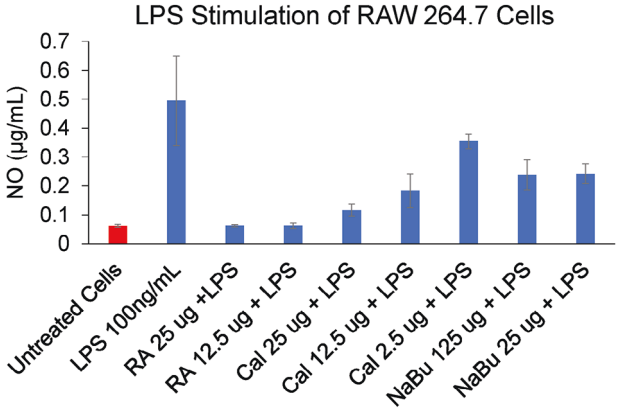

Figure 5. In vitro activity of all-trans retinoic acid (ATRA), sodium butyrate (NaBu), and calcipotriol (Cal) Microneedles on LPS stimulated RAW 264.7 Cells. Griess assay was used to measure the amount of nitric oxide in the supernatant. The microneedles containing ATRA reduced NO concentrations raised by LPS treatment, along with positive controls of Cal and NaBu.

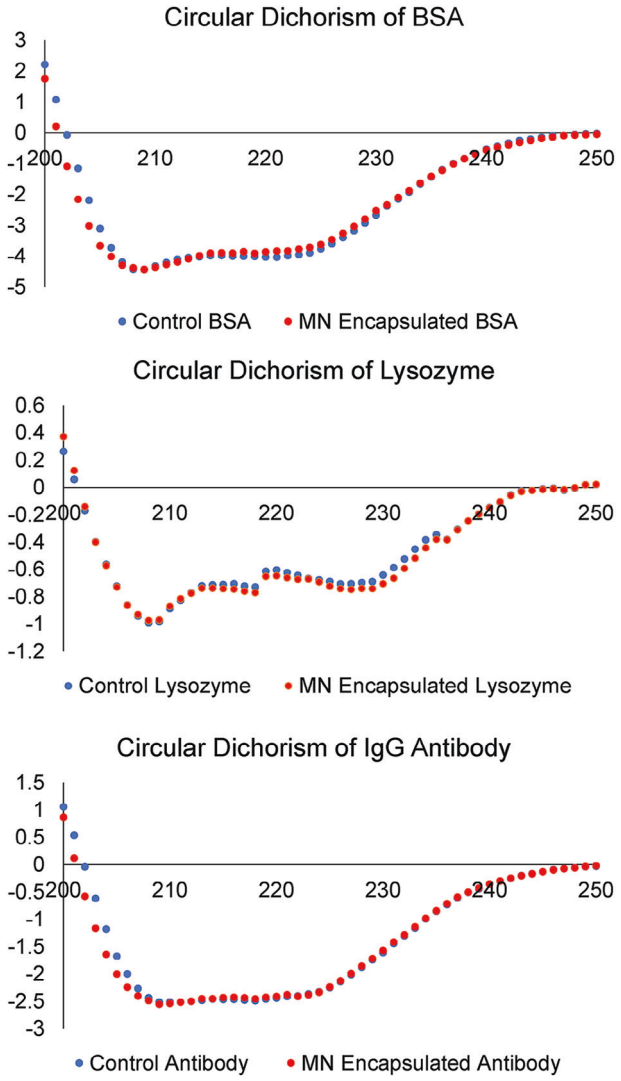

Figure 6. CD Spectra of BSA, lysozyme, and IgG antibody encapsulated in microneedles (MN). Proteins were encapsulated in a layered microneedle patch. Samples were then recovered, PVP filtered off, and the resulting structure was measured.

and microneedles began to dissolve rapidly after penetration. The timed release resulted from the layered structure was measured by a release assay. The release assay showed first order release kinetics for the first layer of CMC with fluorescein, and zero order kinetics for both methylene blue in the second EC layer and TRITC labeled IgG in the PVP layer. CMC rapidly dissolves in water and releases the loaded fluorescein. However, EC does not dissolve. Therefore, the encapsulated methylene blue slowly released into the aqueous environment. Because EC does not form a perfect water repellant barrier, PVP dissolves slowly over time releasing the TRITC labeled IgG.

We showed that through changing the amount of material used, we could adjust the voids left by a particular layer of the microneedles. This was done by altering the volume that was added during microneedle fabrication. It could be extrapolated that by changing the concentrations used for the fabrication the

resulting voids would also be altered. One would also need to account for the viscosity of increased concentration. The effect of viscosity, concentration, volume, and polymers used all impact the void that is left in each individual layer. This multi-parameter control can be further explored later to best enable drug delivery. These therapeutics loaded into each matrix will impact and be impacted by the polymers selected. Thus, individual functionality assays after encapsulation will need to be completed along with release rates.

We tested the ability of a variety of loaded small molecules and proteins to remain active after fabrication. We first examined the anti-inflammatory effect of ATRA, NaBu, and Cal on RAW 264.7 cells stimulated with LPS. This assay showed that even encapsulated in microneedles, the cargo is active and suggests the likelihood of in vivo activity against inflammation. Also, it is important to note the use of both aqueous and organic soluble drugs were used highlighting the flexibility of the system. We validated the ability of the microneedles to encapsulate proteins BSA and lysozyme, two commonly used model proteins. The analysis showed stability of these proteins after encapsulation and release from the microneedles.

This study was the first step in developing a multi-phase microneedle release system. Due to the limited scope of this study and broad range of applications, further characterization of the individual parts will be required prior to clinical use. The current microneedle system requires alternating layers of aqueous and organic solvents and corresponding polymers to limit the mixing of layers. This diversifies the type of drugs that can be used, while simultaneously constraining the order molecules release. Further work is needed on individual solvents and polymers for their effect on layer thickness. The individual properties of polymers must be screened for drug compatibility and timings of release, requiring more initial system optimization. However, this does allow for the adjustable design of an individual needle patch.

This microneedle array is a promising strategy for the release of multiple cargos in future translation work. The tunability of the layer thickness and compatible polymers could be leveraged for the treatment of melanoma, viral diseases, and for vaccines. These scenarios often require multiple doses or therapeutics for optimal efficacy.[22,24] This multilayered microneedle provides a simple approach to drug delivery that can improve the efficacy in these treatments. The ease of fabrication is another advantage of this approach. Future work can optimize these methods for the delivery of drugs specific to a therapy, be it slowing the release of the second and third layer or altering the order of layers fabricated to have zero order kinetics from the first layer. We will continue exploring this system through an in vivo disease model that will further explore the utility of this microneedle system. This study provides a valuable avenue to improve upon already existing therapies or open new single dose options for treatments requiring multiple drugs.

4. Conclusion

We successfully fabricated a multilayered microneedle. This system enables tunable controlled release of multiple therapeutic combinations from a single treatment. This delivers a system to time the release of drugs as needed for optimal therapeutic outcomes. Future work is needed to deliver therapeutics in discrete phases or to further separate the release of agents in the second and third layers. Additional study of the layer thickness to alter release profiles should also be explored as the concept has only been briefly touched on in this work.

5. Experimental Section

Materials: Carboxymethyl cellulose (90 kDa) from Krackeler Scientific (Albany, New York), sterile saline 0.9% (NaCl) from GROWCELLS (Irvine, CA, USA), ethyl cellulose from Grainger (Syracuse, NY, USA), polyvinylpyrrolidone (55 kDa) from Sigma–Aldrich (St. Louis, MO, USA), ethanol, Sylgard 184 Kit from Dow (Midland, MI, USA), bovine serum albumin from VWR (Radnor, PA, USA), fluorescein powder from Thermo Fisher Scientific (Waltham, MA, USA), rhodamine B from BeanTown Chemical (Hudson, NH, USA), RAW 264.7 cells from ATCC (Manassas, VA, USA), cyanine-5 from ApexBio (Houston, TX, USA), ethanol from Decon Labs (PA, USA), LPS (*E. Coli*) from Adipogen Corp MS (San Diego, CA, USA), all-trans retinoic acid (ATRA) from Enzo Life Sciences (Farmingdale, NY, USA), VERIGUIDE OS Resin from Whip Mix (Louisville, KY, USA), isopropyl alcohol from VWR (Radnor, PA, USA), Griess Reagent from Enzo Life Sciences (Farmingdale, NY, USA), lysozyme from MP Biomedicals (Irvine, CA, USA).

Microneedle Fabrication: Microneedles were fabricated through a stepwise process. First microneedle structure was designed in Autodesk Fusion 360 (San Francisco, CA, USA) before being printed on an Asiga MAX X27 (Ann Arbor, MI, USA) with VERIGUIDE OS resin. The 3D printed master molds were removed and were subsequently washed with IPA and fully crosslinked in Flash Cure Asiga Station. After, the PDMS negative molds were generated by mixing Sylgard at a 10:1 polymer to elastomer ratio and cured at 60 °C for 24 h. Master molds were removed, and negative molds were washed with ethanol and dried before use in a vacuum chamber. Microneedles were fabricated by placing material onto the mold followed by degassing the molds, thus filling the mold. The microneedles were dried prior to addition of subsequent layers. This process was then repeated with a second layer chosen to not dissolve the first layer's material. A third layer was then added following the previous steps. Once the final layer was dried a backing layer was applied (3 M Durapore Surgical Tape) to remove the microneedles and for use. (**Figure 7**)

Scanning Electron Microscope (SEM) Imaging: Fabricated microneedles were taken, and sputter coated with 10 nm of Au–Pd prior to imaging with the SEM. SEM images were taken of individual needles and entire patches with this method. Using ImageJ, needle height and width measurements were taken.

Porcine Skin Penetration: Fresh porcine skin was obtained from a local butcher. The skin was stored at 4 °C until the experiment was run. Microneedles loaded with methylene blue were applied by thumb to a section of the skin for 1 min before removal. A light microscope (Nikon) was then used to image the porcine skin and images were captured using an AccuScope attachment. Microneedles were imaged using SEM after insertion into the porcine skin. After microneedle removal, skin was fixed with 4% PFA and 30% sucrose before freezing in Cryomatrix. Samples were sectioned using a Cryostar NX70 followed by H&E staining prior to imaging on a Nikon Eclipse Ti2 inverted microscope.

Microneedle Layer Thickness Control: A two-layer microneedle was generated using the method described in 2.2. Microneedles were generated by using 5% (w/v) EC in chloroform or 5% (w/v) CMC in saline for the first or second layer, alternating the layering order. Volume amounts for the first layer varied from 50 to 150 µL per individual microneedles array. These layers were dried before adding the second layer into the microneedles and again dried. To determine the layer thickness, the first layer of the microneedles was dissolved with either chloroform or distilled water depending on the material used; then the height of the remaining second layer was measured in ImageJ and the corresponding layer heights were measured.

Microneedle Multiphase Release: Microneedles were prepared with three layers. Within these microneedles, three different molecules,

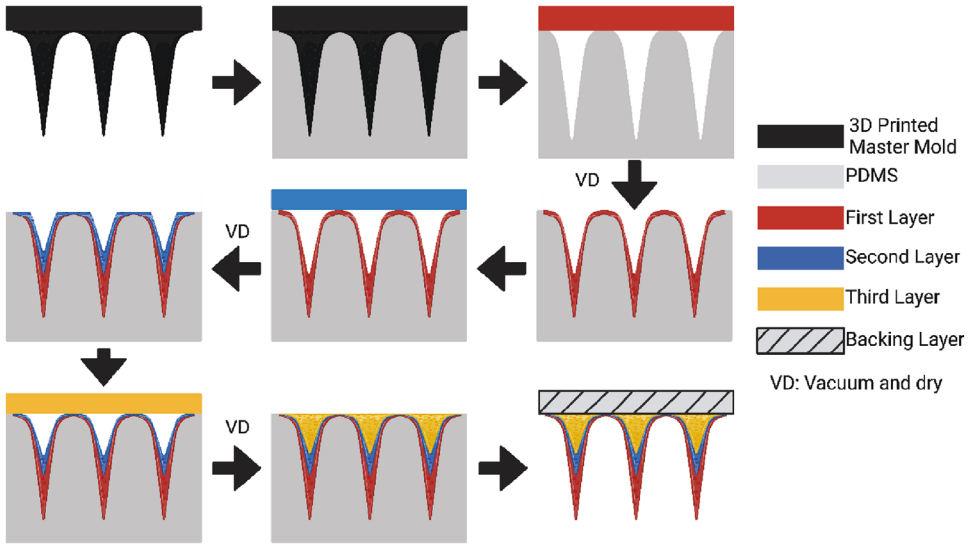

Figure 7. Stepwise fabrication method of multilayered microneedle. This strategy allows for three different distinct layers to be generated in rapid fabrication. The individual layers are made through alternating polymers with varying hydrophilicities to minimize mixing between layers. The resulting microneedle is then removed from the mold after a backing layer is placed over that can be used for in vivo or in vitro applications.

fluorescein, cyanine 5, and rhodamine B were encapsulated into the first, second, and third layers respectively. Once prepared the backs of the microneedles were sealed with cyanoacrylate to prevent exposure from the backend during the study. The microneedles were then placed on the side of scintillation vials, water was then added and stirred gently for the remainder of the study. At predetermined time points aliquots were removed, and fluorescence was measured using a Spectramax M3 microplate reader.

Anti-Inflammatory Activity of All-trans Retinoic Acid (ATRA) Loaded Microneedles in RAW 264.7 Cells Stimulated with Lipopolysaccharide (LPS): A double layered microneedle system was generated using the previously described method. CMC (5%) in saline was used to generate the first layer and the second layer was made from ethyl cellulose with varying amounts of ATRA incorporated into the microneedles to result in 10, 100, and 500 µM solutions within the individual wells. This is to simulate what ATRA release profile would be in a multilayer microneedle.

RAW 264.7 cells were seeded onto a 48 well plate at 4×10^5 cells mL^{-1} and allowed to adhere overnight. The following day microneedles containing ATRA, calcipitriol, or sodium butyrate were added to the cell culture medium and LPS was added to bring the concentration to 100 ng mL^{-1} in each well. The following day, the supernatant was removed from the cells and analyzed for nitric oxide content using the Griess assay. The results were analyzed using the Spectramax M3 microplate reader.

Circular Dichroism of Proteins: A two-layer microneedle was made with PVP and a blank ethyl cellulose layer to simulate the process used for the fabrication of the tri-layer system. Either BSA (1 mg mL^{-1}), lysozyme (1 mg mL^{-1}), or goat IgG (0.05 mg mL^{-1}) loaded into the first layer comprised of PVP. The microneedles were placed into a PBS solution to collect the encapsulated protein. After collection, proteins were isolated from PVP using Sartorius Vivaspin columns. Stock proteins were compared using a JASCO 1500 CD spectrometer. Samples were measured from 250–200 nm, at a rate of 50 nm min^{-1} for three iterations. Following the ellipticity measurements, samples were measured using BeStSel, a documented platform for secondary structure determination, and the resulting helicity and beta-sheet percentages.

Acknowledgements

This work made use of the Cornell Center for Materials Research Shared Facilities which are supported through the NSF MRSEC program (DMR-1719875). The authos would like to thank Dr. Christopher Alabi for his guidance on CD and suggestions for improvements made to the microneedles.

Conflict of Interest

The authors declare no conflict of interest.

Data Availability Statement

The data that support the findings of this study are available from the corresponding author upon reasonable request.

Keywords

antibody, drug delivery, microneedles, timed release

Received: September 21, 2023
Revised: November 13, 2023
Published online: December 10, 2023

[1] M. S. Alqahtani, M. Kazi, M. A. Alsenaidy, M. Z. Ahmad, *Front Pharmacol* **2021**, *12*, 618411.
[2] M. R. Prausnitz, R. Langer, *Nat. Biotechnol.* **2008**, *26*, 1261.
[3] A. Alkilani, M. T. Mccrudden, R. Donnelly, *Pharmaceutics* **2015**, *7*, 438.
[4] J. H. Jung, S. G. Jin, *J Pharm Investig* **2021**, *51*, 503.
[5] W. Y. Jeong, M. Kwon, H. E. Choi, K. S. Kim, *Biomater. Res.* **2021**, *25*, 24.
[6] A. Z. Alkilani, J. Nasereddin, R. Hamed, S. Nimrawi, G. Hussein, H. Abo-Zour, R. F. Donnelly, *Pharmaceutics* **2022**, *14*, 1152.
[7] S. Park, K. Lee, W. Ryu, *Expert Opin. Drug Delivery* **2022**, *19*, 1115.
[8] Z. Faraji Rad, P. D. Prewett, G. J. Davies, *Beilstein J. Nanotechnol.* **2021**, *12*, 1034.
[9] T. Waghule, G. Singhvi, S. K. Dubey, M. M. Pandey, G. Gupta, M. Singh, K. Dua, *Biomed. Pharmacother.* **2019**, *109*, 1249.

[10] H. S. Min, Y. Kim, J. Nam, H. Ahn, M. Kim, G. Kang, M. Jang, H. Yang, H. Jung, *Biomater Adv* **2023**, *145*, 213248.
[11] X. Hong, Z. Wu, L. Chen, F. Wu, L. Wei, W. Yuan, *Nano-Micro Lett.* **2014**, *6*, 191.
[12] P. Makvandi, M. Kirkby, A. R. J. Hutton, M. Shabani, C. K. Y. Yiu, Z. Baghbantaraghdari, R. Jamaledin, M. Carlotti, B. Mazzolai, V. Mattoli, R. F. Donnelly, *Nano-Micro Lett.* **2021**, *13*, 93.
[13] R. Neupane, S. H. S. Boddu, J. Renukuntla, R. J. Babu, A. K. Tiwari, *Pharmaceutics* **2020**, *12*, 152.
[14] W. Li, R. N. Terry, J. Tang, M. R. Feng, S. P. Schwendeman, M. R. Prausnitz, *Nat. Biomed. Eng.* **2019**, *3*, 220.
[15] M.-C. Chen, M.-H. Ling, K.-Y. Lai, E. Pramudityo, *Biomacromolecules* **2012**, *13*, 4022.
[16] J. Yu, Y. Zhang, Y. Ye, R. Disanto, W. Sun, D. Ranson, F. S. Ligler, J. B. Buse, Z. Gu, *Proc. Natl. Acad. Sci. USA* **2015**, *112*, 8260.
[17] P. Dosta, N. Puigmal, A. M. Cryer, A. L. Rodríguez, E. Scott, R. Weissleder, M. A. Miller, N. Artzi, *Theranostics* **2023**, *13*, 1.
[18] K. T. M. Tran, T. D. Gavitt, T. T. Le, A. Graichen, F. Lin, Y. Liu, E. R. Tulman, S. M. Szczepanek, T. D. Nguyen, *Adv. Mater. Technol.* **2023**, *8*, 2200905.
[19] T. Sheng, B. Luo, W. Zhang, X. Ge, J. Yu, Y. Zhang, Z. Gu, *Adv. Drug Delivery Rev.* **2021**, *179*, 113919.
[20] Y. Hu, N. Liu, B. Cheng, Y. Tan, L. Wen, H. Yuan, F. Hu, *OncoTargets Ther.* **2016**, *7*, 83258.
[21] H. Duan, C. Liu, Y. Hou, Y. Liu, Z. Zhang, H. Zhao, X. Xin, W. Liu, X. Zhang, L. Chen, M. Jin, Z. Gao, W. Huang, *ACS Appl. Mater. Interfaces* **2022**, *14*, 10102.
[22] T. Rager, A. Eckburg, M. Patel, R. Qiu, S. Gantiwala, K. Dovalovsky, K. Fan, K. Lam, C. Roesler, A. Rastogi, S. Gautam, N. Dube, B. Morgan, S. M. Nasifuzzaman, D. Ramaswami, V. Gnanasekar, J. Smith, A. Merchant, N. Puri, *Cancers* **2022**, *14*, 3779.
[23] X. Jiang, P. B. Lillehoj, *Microsyst. Nanoeng.* **2020**, *6*, 1.
[24] Z. A. Shyr, Y.-S. Cheng, D. C. Lo, W. Zheng, *Drug Discov Today* **2021**, *26*, 2367.

